AIAA 81-0651R

Wind-Tunnel Study of the Flutter Characteristics of a Supercritical Wing

R. Houwink,* A. N. Kraan,† and R. J. Zwaan‡
National Aerospace Laboratory, Amsterdam, the Netherlands

A wind-tunnel flutter test on a supercritical wing model is described. Objectives of the test were to investigate the transonic dip and to make comparisons with calculated flutter characteristics in which a quasi-three-dimensional transonic theory was used. The beginning of a transonic dip was measured and a satisfactory agreement with theory could be found. An additional flutter instability in the bottom of the transonic dip could be correlated with the loss of transition strip effectivity at low Reynolds numbers.

Nomenclature

a,b = correction factors [Eqs. (2)]
c = chord
C_{ℓ_0} = sectional steady lift coefficient
C_L = wing lift coefficient
f = frequency
g = damping coefficient
k = reduced frequency (related to semichord)
k = sectional unsteady lift coefficient, k_{2D}, k_{3D}
m = sectional unsteady moment coefficient (related to quarterchord), m_{2D}, m_{3D}
M_∞ = Mach number
P_0 = stagnation pressure
q = generalized coordinate
Re_c = Reynolds number related to mean aerodynamic chord
x_t = position of transition strip
α = wing angle of incidence
Λ = (mean) sweep angle

Subscripts

e = equivalent two-dimensional
B = wing bending
F = flutter
R = wing rotation

Introduction

In recent years the supercritical wing concept for transport aircraft has given rise to considerable concern about the detrimental effects which the optimized aerodynamic efficiency of the supercritical wing may have on the flutter characteristics. At present only limited information is available on this subject. In Ref. 1, flutter characteristics of a supercritical and a conventional wing, measured in the wind tunnel have been compared, especially in the region of the so-called transonic dip. Reference 2 presents calculation methods for unsteady transonic airloads based on transonic corrections of the subsonic doublet-lattice method. Results of flutter calculations are presented and successfully correlated with measured data for the same wing as considered in Ref. 1.

Also at NLR, theoretical and experimental investigations have been initiated to penetrate the area of transonic flutter characteristics of supercritical wings. The interest of NLR is directed to a wing with larger airfoil thickness and less sweep than in Ref. 1, i.e., a wing with a more or less two-dimensional character of the flow over a considerable part of the wing span.

Recently at NLR a flutter test was performed on the half-model of a supercritical transport-type wing that was elastically clamped to the wind-tunnel side wall. Variables were Mach number, stagnation pressure, and wing incidence. This wing was considered as a study model and did not represent the flutter characteristics of any existing aircraft design. The test objectives were 1) the exploration of the transonic dip in the flutter boundaries, and 2) the evaluation of a method to calculate airloads on an oscillating three-dimensional wing in transonic flow by comparing measured and calculated flutter characteristics of the model.

The calculation method is the so-called quasi-three-dimensional method which has been developed recently at NLR for wings with a relatively large aspect ratio. In brief, the method combines a calculation method for airloads on oscillating two-dimensional wings in transonic flow, with three-dimensional corrections due to wing span and taper obtained from two- and three-dimensional subsonic lifting surface theory. A further explanation is given in a later section of this paper.

A more direct validation of the quasi-three-dimensional method would preferably be performed by comparison of experimental and theoretical pressure distributions on an oscillating three-dimensional supercritical wing. Such an investigation, however, would require a rather complicated wind-tunnel model. Because of time and cost only a flutter model was tested.

In this paper the test setup and the main results of the flutter test are presented. Further, an analysis of the results is given and a comparison is made with calculated results.

Test Setup

The flutter test was carried out in the NLR transonic wind-tunnel HST, of which the Mach number can be increased to $M_\infty = 1.35$, while the stagnation pressure can be varied between $P_0 = 12.5$ and 400 kPa. The rectangular test section measures 2.00 m wide and 1.60 m high and is fitted at upper and lower wall with longitudinal slots with open area ratio of 0.125.

The test object was a half-model of a supercritical wing with an aspect ratio of 11 and an airfoil thickness distribution of 16% at the root to 11.5% at the tip (Fig. 1). The sweep angle at 25% chord (outer wing part) is 16 deg. The design Mach number is 0.75. The wing model was made of solid duraluminum and was fixed to a turntable in the wind-tunnel side wall by means of a torsional spring (Fig. 2). A half-body representing the fuselage was also fixed to the turntable. Finally, a transition strip of carborundum grains (grit 220)

Presented as Paper 81-0651 at the AIAA Dynamics Specialists Conference, Atlanta, Ga., April 9-10, 1981; submitted April 27, 1981; revision received Oct. 6, 1981.

*Research Engineer, Department of Aeroelasticity; presently employed by Dutch Civil Aviation Department.
†Senior Research Engineer, Department of Aeroelasticity.
‡Head, Department of Aeroelasticity.

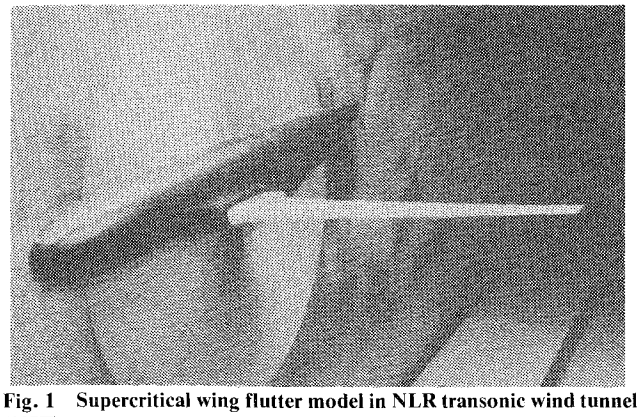

Fig. 1 Supercritical wing flutter model in NLR transonic wind tunnel (HST).

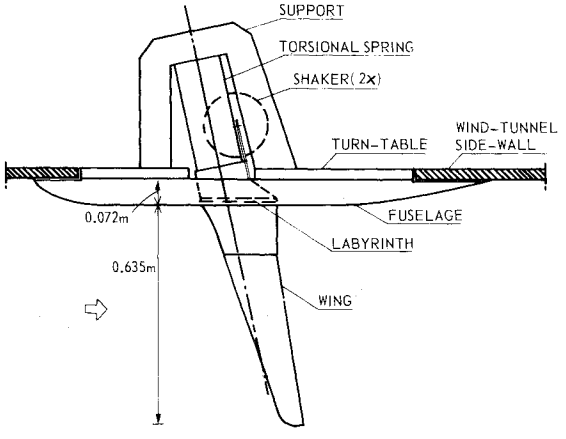

Fig. 2 Test setup for supercritical wing flutter model.

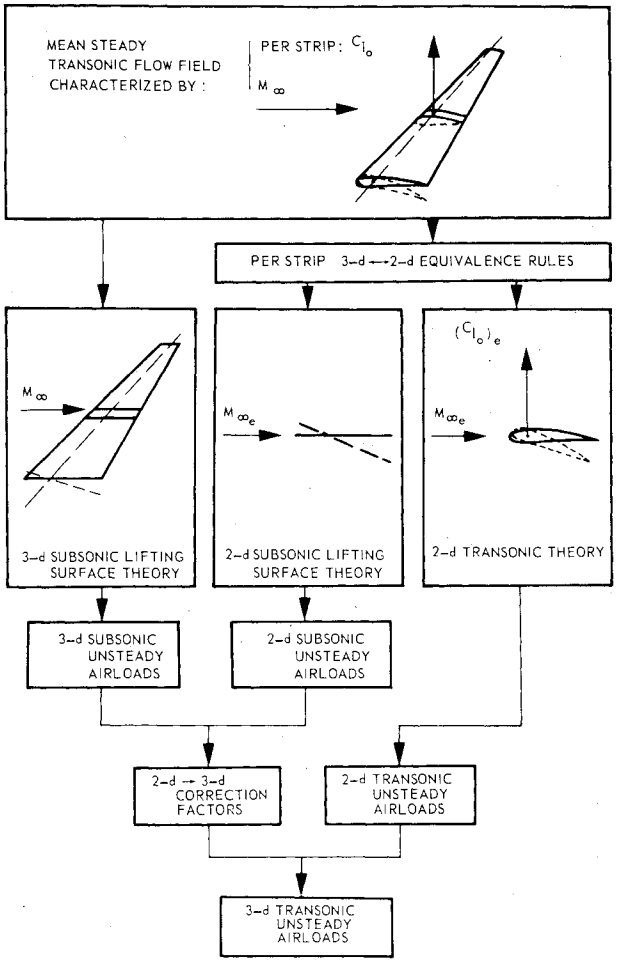

Fig. 3 Flow diagram of quasi-three-dimensional method.

was installed at 5% chord position on the upper and lower wing surface.

In designing the spring, a compromise had to be found between its strength, which had to be sufficient to withstand the mean aerodynamic loading of the wing, and its stiffness which should especially satisfy the following two requirements. First, with wing bending and spring torsion as degrees of freedom, flutter should occur within the operational limits of the wind tunnel. In order to find a well-defined flutter boundary, the type of flutter should not be too mild. Second, the flutter frequencies should be low enough so that strong transonic effects could be expected. The design of the spring led to an X-shaped bar which was rigid in bending and relatively weak in torsion. This modeling of the spring gave the flutter model its character of a study model, without the intention of scaling any existing aircraft design.

Excitation of the model was provided by wind-tunnel turbulence and by frequency sweeps from two shakers. The model response was measured by strain-gage bridges on the spring flanges. After data reduction and processing, the responses were presented as analog signals and as power spectral density plots from which frequencies and damping values were derived by means of a curve-fitting procedure.

To enable the approach of the flutter boundary to be as close as possible, the two shakers were also able to act as a flutter damper. This device was a feedback system in which the signals of the torsion bridge and the maximum-stress bridge were used. Once a preset amplitude level was exceeded, the torsion signal activated the shakers with a 90-deg phase shift.

Test Procedure

The test procedure included runs at constant Mach number and increasing stagnation pressure, as well as runs at constant stagnation pressure and increasing Mach number. The runs were performed up to the flutter boundaries. At each subcritical measuring point, frequency and damping were measured. This procedure was performed for three angles of incidence: $\alpha_0 = -0.45$, 0.10, and 0.75 deg, which could be adjusted by rotating the turntable.

With the strain-gage bridges on the spring, the mean aerodynamic loading on the wing was also measured. This information was used to make allowance for the spring deformation under the mean aerodynamic loading. For this purpose, use was made of results of steady tests on an earlier model of the wing. The steady data also provided information about the true angle of attack during the flutter test.

Outline of the Quasi-Three-Dimensional Method

The method for calculating the unsteady airloads consists of a series of calculation steps indicated in the flow diagram of Fig. 3.

The idea underlying the quasi-three-dimensional method is that, for each streamwise wing section, its unsteady loading can be subdivided into two parts: 1) airloads on a similar section of a swept wing of zero taper and infinite span; 2) corrections for the three-dimensional effects of taper and aspect ratio of the actual wing.

The basic assumption is that, for a high-aspect-ratio wing in transonic flow, the transonic effects (of thickness and incidence) on the three-dimensional corrections (part 2) are negligible relative to the transonic effects on the sectional airloads (part 1). The latter "equivalent two-dimensional" airloads can be determined using a two-dimensional transonic theory, taking into account the well-known two-dimensional equivalence rules for a wing with (mean) sweep angle Λ:

$$(M_\infty)_e = M_\infty \cos\Lambda \qquad (1a)$$

$$(C_{\ell_0})_e = C_{\ell_0}/\cos^2\Lambda, \text{ etc.} \quad (1b)$$

The three-dimensional corrections can be determined using two- and three-dimensional subsonic linear theory. For the present wing, the above principles, illustrated in Fig. 3, were made the basis for the following procedure. First, a mean effective sweep angle was chosen (about halfway between the leading and the trailing edge). The wing was divided into a number of streamwise strips, and for each combination of Mach number, sectional lift coefficient, vibration mode, and reduced frequency realized during the test, the equivalent two-dimensional conditions were determined. Second, it was assumed that also at transonic flow conditions the unsteady airloads behaved in an approximately linear way, and therefore could be superposed like in subsonic flow.

For each strip, unsteady lift and moment coefficients were determined using tables containing results of two-dimensional subsonic lifting surface theory and two-dimensional transonic small perturbation theory for standard pitching and plunging motions. The transonic method is the LTRAN2-NLR code developed at NLR,[3] a higher frequency version of the original LTRAN2 code. The tables with transonic coefficients were computed for one characteristic wing section and for various Mach numbers, reduced frequencies, and lift coefficients $(C_{\ell_0})_e$. A crucial step now was matching the steady pressure distributions corresponding to the tables with the mean steady pressure distributions which existed during the flutter test. Because only the angle of attack of the flutter model was measured, the corresponding steady pressure distributions were obtained using results of steady tests on an earlier pressure model of the present wing. As a basis for matching, the best possible agreement of shock location and shock strength at 70% span and at the same equivalent Mach number M_{∞_e} was chosen.

This matching yields a relation between the experimental and theoretical values of $(C_{\ell_0})_e$. The matching procedure was verified previously by calculations and by a comparison with wind-tunnel results of quasi-steady airloads for a supercritical wing of the same type as the present wing. After matching, the corresponding steady lift coefficient $(C_{\ell_0})_e$ was used to interpolate the transonic coefficients in the tables.

In the following step, three-dimensional subsonic unsteady lifting surface theory was applied from which sectional lift and moment coefficients were derived. These coefficients were combined with the corresponding results of two-dimensional subsonic theory to generate the following sectional correction factors, which accounted for the three-dimensional effect:

$$a = (k_{3D}/k_{2D})_{subs} \quad (2a)$$

$$b = (m_{3D}/k_{3D} - m_{2D}/k_{2D})_{subs} \quad (2a)$$

The calculation of these factors, which are complex, was repeated for each strip, Mach number, reduced frequency, and mode shape. The correction factors were applied to the two-dimensional transonic coefficients:

$$k_{3D} = ak_{2D} \quad (3a)$$

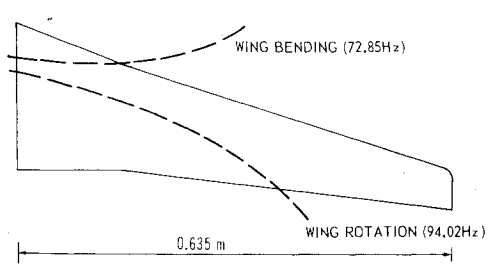

Fig. 4 Natural frequencies and nodal line positions.

$$m_{3D} = a(m_{2D} + bk_{2D}) \quad (3b)$$

These expressions make clear that factor a contains a correction on the two-dimensional sectional unsteady lift coefficient, while factor b represents the shift of the center of pressure due to three-dimensional effects.

The modified coefficients were finally used to calculate the generalized aerodynamic forces required for the flutter calculations.

Experimental Results

Vibration Tests

Two vibration modes controlled the flutter characteristics: the fundamental wing bending mode and a rotational mode about the spring axis. The nodal lines are indicated in Fig. 4. The modal data, including generalized masses, were measured in the wind tunnel prior to the flutter tests. The frequency of the third natural mode was measured at 210 Hz.

Flutter Boundaries

The flutter boundaries for three angles of incidence are presented in Fig. 5a, and the corresponding flutter frequencies in Fig. 5b. As a reference, results of three-dimensional subsonic theory are also given. Concerning the flutter boundaries, the following observations can be made.

1) Up to $M_\infty = 0.65$, all three flutter boundaries coincide and there is hardly any influence of the angle of incidence. Obviously the flow can be considered subsonic. There is a slight unconservativism in the calculated flutter boundary.

2) At increasing Mach numbers beyond $M_\infty = 0.65$, the measured flutter boundaries diverge, depending on the angle of incidence. The decrease of P_{0_F} is strongest for the highest wing incidence. This is not surprising, since transonic effects can be expected to increase with incidence. The calculated flutter boundary becomes increasingly unconservative. This reflects the increasing transonic efficiency of the wing. A similar effect has been found in Ref. 1.

3) The flutter boundaries show the first half of the transonic dip, but, unexpectedly, at low stagnation pressures the boundaries turn back to lower Mach numbers. At $P_0 \approx 40$ kPa, runs were made with increasing Mach number without

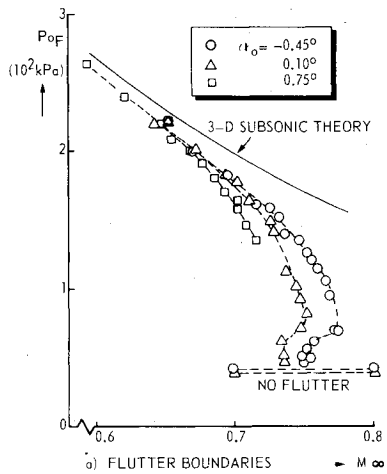

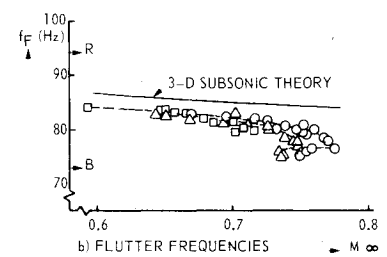

Fig. 5 Measured flutter boundaries and frequencies; B = wing bending, R = wing rotation.

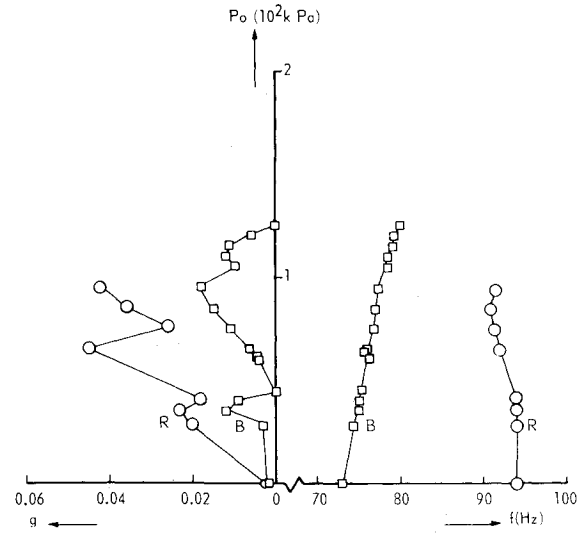

Fig. 6 Flutter diagram for $M_\infty = 0.75$ and $\alpha_0 = -0.45$ deg; B = wing bending, R = wing rotation.

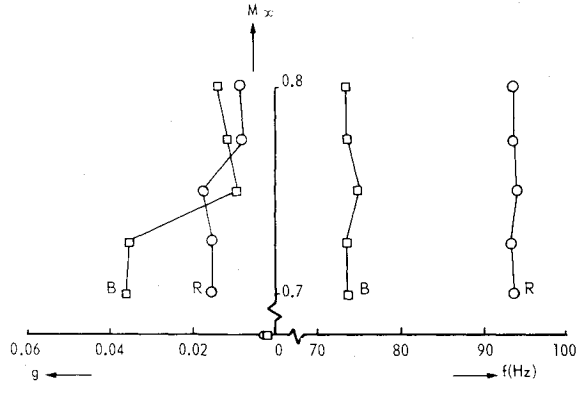

Fig. 7 Flutter diagram for $P_0 = 40$ kPa and $\alpha_0 = -0.45$ deg; B = wing bending, R = wing rotation.

encountering zero damping. These results indicate that some sort of transonic dip should be present but of a somewhat different shape than has been shown in Ref. 1.

The flutter frequency curves, Fig. 5b, start at low Mach numbers nearly in the middle of the frequency interval between wing bending and wing rotation, but shift at higher Mach numbers to the wing bending frequency. The shift is not predicted by the calculated curve.

The test points at low stagnation pressure required a long time to evacuate the wind tunnel and so it was considered too dangerous to pass the dip underneath and then to increase the Mach number in order to determine the other side of the dip.

Flutter Diagrams

The type of flutter is revealed by the flutter diagrams. In Fig. 6 the frequencies and damping values are presented for a stagnation pressure run at $M_\infty = 0.75$ and $\alpha_0 = -0.45$ deg. Two observations are made. First, the frequency curves approach each other gradually, while the wing bending branch becomes unstable and the wing rotation branch becomes heavily damped. This behavior points very clearly to a case of classical two-degrees-of-freedom flutter. Second, at lower stagnation pressures the frequency difference is still large, while the damping curve of wing bending experiences a local decrease of damping. At $P_0 = 45$ kPa the damping of wing bending even becomes zero. Obviously this behavior reflects a one-degree-of-freedom-type oscillation of the model.

Because of the peculiarities at low stagnation pressures, additional Mach number runs were made. An example of such

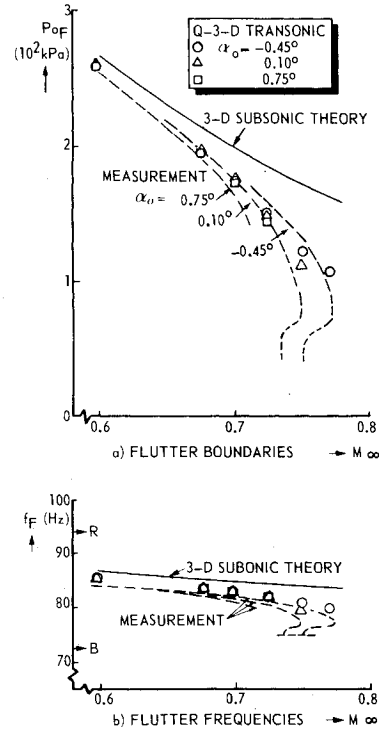

Fig. 8 Comparison of calculated flutter characteristics using the quasi-three-dimensional method and experimental results; B = wing bending, R = wing rotation.

a run at $P_0 = 40$ kPa is given in Fig. 7. (At $P_0 = 45$ kPa the run was very short.) The frequency difference remains nearly constant, while the damping branch of wing bending shows a local decrease near $M_\infty = 0.75$. Also, this result makes the conclusion plausible that for low stagnation pressures a one-degree-of-freedom motion occurs.

A possible explanation of this instability at low stagnation pressures will be given in a following section. The flutter boundaries at these low pressures, however, do not look very well suited to verify the quasi-three-dimensional method.

Comparison of Measured and Calculated Flutter Characteristics

The flutter calculations were performed with a version of the p-k method in which the stagnation pressure could be varied at constant Mach number. The two degrees of freedom taken into account were the wing bending and wing rotation modes as measured at wind-off.

A comparison of results calculated with the quasi-three-dimensional airloads and experimental results is presented in Fig. 8. At subsonic Mach numbers a very good agreement exists. The difference between the results of quasi-three-dimensional theory and of three-dimensional subsonic theory is due to the effect of wing thickness on the unsteady aerodynamic forces.

In the transonic range the calculated and experimental results still agree reasonably well, although the calculated flutter boundaries in Fig. 8a reflect a smaller influence of the angle of incidence than the experimental boundaries. This may be caused by one or all of the following: the quasi-three-dimensional method; viscous effects; and uncertainty about the mean steady flowfield. However, further analysis is difficult because aerodynamic data were not measured during the flutter test. Nevertheless, in comparison with the three-dimensional subsonic curve (Fig. 8a) the quasi-three-dimensional curves show a definite improvement.

A comparison of the frequency and damping curves (Fig. 9) shows a satisfactory agreement. As could be expected, the characteristics of the bending mode damping curve at low stagnation pressures are not predicted by calculation.

Theory also provides the development of the flutter mode shape. In Fig. 10 the amplitude ratio of the bending and the

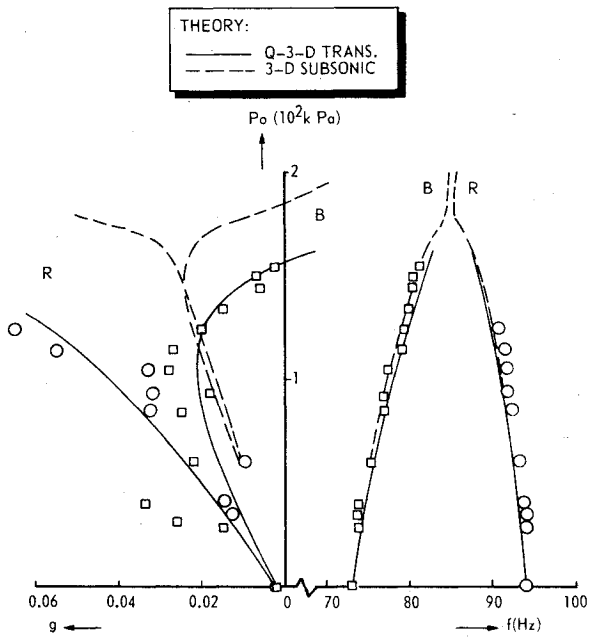

Fig. 9 Comparison of calculated and measured flutter diagram for $M_\infty = 0.725$ and $\alpha_0 = -0.45$ deg; B = wing bending, R = wing rotation.

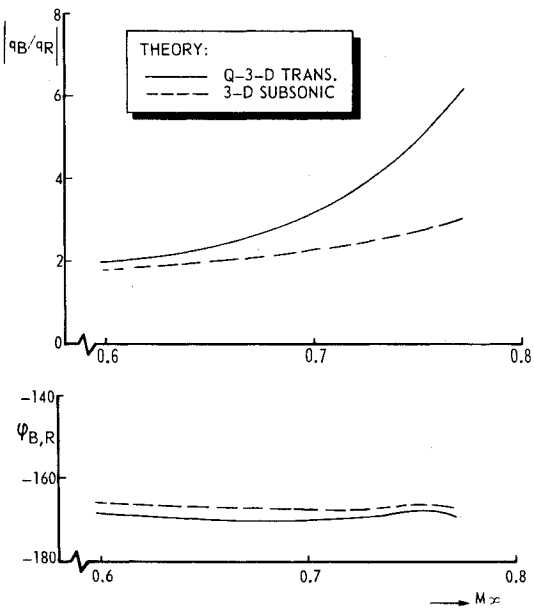

Fig. 10 Calculated flutter mode shape for $\alpha_0 = -0.45$ deg.

rotation mode is presented as modulus and phase. As Mach number increases, the bending mode starts to dominate the rotation mode. This trend is obviously amplified by transonic effects, which indicates that a continuation of flutter calculations for still higher Mach numbers would yield a nearly one-degree-of-freedom flutter mechanism in wing bending. This expectation is also founded on the results of the studies in Refs. 4 and 5.

Explanation of the Instability at Low Stagnation Pressures

Concerning the deviating behavior of the flutter boundary at low stagnation pressures, it was not expected that flow separation would be a dominant factor since during steady pressure tests on an earlier model of the wing the buffet boundary was found to lie at considerably higher Mach numbers. A more likely explanation was that the transition

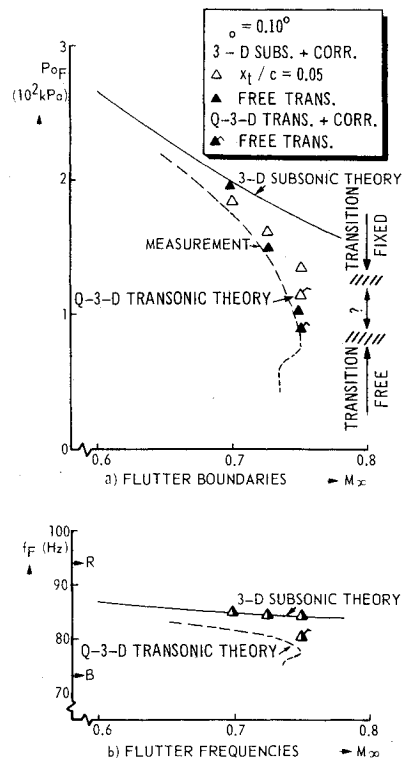

Fig. 11 Comparison of measured flutter boundaries and frequencies with calculations including quasi-steady corrections; B = wing bending, B = wing rotation.

strip had become ineffective at low stagnation pressures, consequently leading to a variable transition point location and a deviation of the unsteady airloads. The strip used in the flutter test had an optimized roughness for $Re_{\bar{c}} = 2 \times 10^6$, corresponding to about $P_0 = 125$ kPa at $M_\infty = 0.75$. For low values, $P_0 \approx 50$ kPa corresponding to $Re_{\bar{c}} \approx 1 \times 10^6$, this strip might have become ineffective. To verify this presumption, an additional steady pressure test was performed, including measurements at $Re_{\bar{c}} = 1 \times 10^6$ and 2×10^6, with a transition strip at 5% chord, optimized for $Re_{\bar{c}} = 2 \times 10^6$. Indeed, the pressure distributions and the quasi-steady airloads at the lower Reynolds number were characteristic for free transition and differed considerably from the results at the higher Reynolds number. For example, at $M_\infty = 0.75$ the value of C_{L_α} at the lower Reynolds number was about 10% more than at the higher Reynolds number.

To estimate the consequences for the flutter boundaries, flutter calculations were made in which all aerodynamic forces according to three-dimensional subsonic theory were multiplied by the ratio (C_{L_α} from steady pressure test)/(C_{L_α} from three-dimensional subsonic theory at $k = 0$). The results are shown in Fig. 11 for $\alpha_0 = 0.10$ deg. The flutter mechanism remains the same, but the drop of the flutter boundary becomes stronger for the case of free transition (Fig. 11a). The flutter frequency, however, is not affected (Fig. 11b), indicating that the flutter mode shape is essentially the same as that calculated with three-dimensional subsonic theory. The drop of the flutter boundary is obviously not accompanied by the increased domination of the bending mode as predicted by the flutter calculations using the quasi-three-dimensional method. This means that results of transonic flutter calculations based on subsonic airloads corrected with quasi-steady transonic factors derived from wind-tunnel tests should be viewed with caution.

In a similar way the airloads according to quasi-three-dimensional theory were corrected. Assuming equivalence of unsteady airloads calculated with quasi-three-dimensional theory and wind-tunnel airloads corresponding to fixed transition, the factor was taken as (C_{L_α} at free transition)/(C_{L_α} at fixed transition). The flutter results are given in Fig. 11. In this case both flutter pressure and flutter

frequency drop off. Also in Fig. 11a, the regions of presumed strip effectivity have been indicated. For $M_\infty = 0.75$ the shift of the flutter boundary due to the correction is large enough to admit the conclusion that the free transition character most probably prevailed.

Finally, an analysis was made of wind-tunnel data obtained at NLR for oscillating airfoils in transonic flow at fixed as well as at free transition. At flow conditions comparable to those at the transonic dip, the phase lag at free transition turned out to be some 10 deg larger. Subsequent flutter calculations in which all airloads were given only a few degrees additional phase lag showed a considerable drop of the flutter boundary.

The results of the above trend study give rise to the idea that each measured flutter boundary in the present test can be divided into two parts. The first part is governed by airloads for fixed transition and the second part is governed by airloads with varying transition point location. The latter occurs at low stagnation pressures and slightly lower Mach numbers. Transition from the first to the second part takes place obviously just below $P_0 = 80$ kPa.

It is clear that a reliable quantitative analysis of this additional instability would require more complete aerodynamic data. It is also clear, however, that the change in flutter behavior at low Reynolds numbers had to do with the problem of scaling boundary layer effects properly and that this instability would not have been encountered if the transition strip had been effective at all flow conditions.

Considering the practical meaning of the flutter results with ineffective transition strip, one should realize that according to experience from steady transonic tests, artificial transition is mandatory for Reynolds numbers below 1×10^7 to obtain data which are representative for real flight conditions. When the transition strip becomes ineffective, of course the actual Reynolds numbers of the test hold. Because full-scale Reynolds numbers are usually much higher, the additional instability in the transonic dip is less meaningful.

Conclusions

A wind-tunnel flutter test was performed on a supercritical wing model which was made to flutter within the operational limits of the tunnel. A study of the measured flutter characteristics and the comparison with calculated results lead to the following conclusions.

1) In the flutter test, the beginning of a transonic dip was found. A complete dip could not be determined owing to an additional flutter instability in the bottom of the dip.

2) The experimental flutter boundaries bend to lower stagnation pressures with increasing wing incidence. In a more general sense, this result emphasizes the need to perform transonic flutter tests at different wing incidences.

3) The beginning of the transonic dip and the influence of wing incidence was predicted by the flutter calculations in which the quasi-three-dimensional method for unsteady transonic flow was used. A satisfactory agreement of experiment and theory was shown, although the influence of wing incidence was underestimated by theory.

4) In the transonic dip, both experiment and theory indicate a nearly one-degree-of-freedom flutter of the wing bending mode.

5) The occurrence of an additional flutter instability in the bottom of the transonic dip could be correlated with an insufficient effectivity of the transition strip at low stagnation pressures, leading to a considerable change in the unsteady airloads. The type of flutter mechanism remains the same, but the flutter boundary shifts to somewhat lower Mach numbers. This experience demonstrates that in order to represent the transonic dip of an actual aircraft in the wind tunnel, full transition strip effectivity in all relevant flow conditions is required.

Acknowledgments

This investigation was carried out under contract for the Netherlands Agency for Aerospace Programs and in cooperation with the Netherlands Aircraft Factories Fokker B. V.

References

[1] Farmer, M. G. and Hanson, P. W., "Comparison of Supercritical and Conventional Wing Flutter Characteristics," *Proceedimgs of the AIAA/ASME/SAE 17th Structures, Structural Dynamics, and Materials Conference,* King of Prussia, Pa., May 1979.

[2] McGrew, J. A., Giesing, J. P., Pearson, M., Zuhuruddin, K., Schmidt, M. E., and Kalman, T. P., "Supercritical Wing Flutter," AFFDL-TR-78-37, March 1978.

[3] Houwink, R. and van der Vooren, J., "Results of an Improved Version of LTRAN2 for Computing Unsteady Airloads on Airfoils Oscillating in Transonic Flow," *AIAA Journal*, Vol. 18, Aug. 1980, pp. 1008-1010.

[4] Isogai, K., "On the Transonic-Dip Mechanism of Flutter of a Sweptback Wing," *AIAA Journal,* Vol. 17, July 1979, pp. 793-795.

[5] Isogai, K., "Numerical Study of Transonic Flutter of a Two-Dimensional Airfoil," National Aerospace Laboratory TR-617 T, July 1980.